Shear-Induced Crystallization of Poly(butylene terephthalate): A Real-Time Small-Angle X-ray Scattering Study

Liangbin Li* and Wim H. de Jeu

FOM-Institute for Atomic and Molecular Physics, Kruislaan 407, 1098 SJ, Amsterdam, The Netherlands

Received February 26, 2004; Revised Manuscript Received May 14, 2004

ABSTRACT: The shear-induced crystallization behavior of poly(butylene terephthalate) (PBT) has been investigated by in-situ small-angle X-ray scattering at temperatures of 198, 203, and 208 °C as well as by ex-situ atomic force microscopy. Increasing the shear rate and/or the shear strain enhances the crystallization kinetics. The acceleration of the crystallization saturates with increasing shear rate. A pronounced effect of the shear field on the Avrami exponent is observed at 198 °C but not at 203 and 208 °C, even though at the latter temperatures the relative reduction of the crystallization time induced by the shear is twice the value at 198 °C. Compared to some other polymers like isotactic polypropylene, the shear field leads only to a weak orientation of the PBT crystals. The Avrami exponent and the orientation induced by the shear field are interpreted on the basis of a microshish model. Microshish structures are due to the breaking up of shear-induced row nuclei at high temperatures. Finally, the shear field is found to lead to a decrease of the long period.

Introduction

Knowledge of flow-induced crystallization in the polymer melt is essential to control the final properties of products during industrial processing methods such as extrusion, injection, and blow molding. Nevertheless, no satisfactory molecular theory exists that can describe polymers under flow.[1−3] However, several points regarding shear-induced crystallization of polymers are well established:[4] (i) Shear accelerates the crystallization kinetics and, under severe conditions, changes the semicrystalline morphology from spherulites to crystallites oriented in the flow direction. (ii) The enhancement of the crystallization kinetics is attributed to an increase in the nucleation rate caused by distortions of the polymer chains in the melt. This conclusion is based on studies of the nucleation density, the induction time for nucleation, and the crystal growth rate. (iii) The molecular weight and the molecular weight distribution have a pronounced effect. High-molecular-weight species play an important role in orienting the melt and in the observed enhancement of the crystallization kinetics.[4−8]

Most studies of the effect of shear on the crystallization behavior of polymer melts are limited to polyolefins, especially isotactic polypropylene.[4−26] Less work has been dedicated to engineering plastics, even though from a commercial point of view these materials have the same importance as commodity plastics.[27,28] We attribute this difference to the difficulty of handling in-situ experiments of most engineering plastics due to the high melting temperatures and the associated possibility of degradation. Consequently, reports on orientation-induced crystallization are often limited to low-temperature drawing or stretching of solid samples instead of shearing of the polymer melt.[29−31] Unfortunately, knowledge from polyolefins cannot be directly applied to engineering plastics such as poly(ethylene terephthalate) (PET) and poly(butylene terephthalate) (PBT). One reason is the difference in chain rigidity, which can strongly influence the relaxation process. Although stress relaxation can generally be described by a single power law decay $t^{-\alpha}$, the exponent α varies from $^1/_2$ for flexible chains to $^5/_4$ for stiff ones.[32] Moreover, a transition from an isotropic to a nematic phase can occur in the melt of semirigid chain polymers upon passing a critical rigidity.[33] Finally, compared to polyolefins, usually different methods of synthesis are used for engineering plastics, which can result in differences in molecular weight as well as in its distribution. As mentioned above, these factors strongly affect the crystallization behavior under shear.

In this work we report on in-situ small-angle X-ray scattering used to investigate the crystallization behavior of PBT. PBT is a typical engineering plastic with semirigid chains, whose crystallization behavior under quiescent condition has been well studied. The morphology of PBT spherulites has been investigated by optical microscopy, small-angle light scattering, and transmission electron microscopy.[34−36] Hou et al. studied the temperature dependence of both the lattice parameters and the lamellar spacing with in-situ X-ray scattering.[37] Hsiao et al. reported about the isothermal crystallization of PBT and its composites with glass fibers using in-situ small-angle X-ray scattering (SAXS).[38] This paper reports on the influence of a shear field on the crystallization kinetics as well as on the morphology development of PBT. Both shear rate and strain lead to a pronounced enhancement of the crystallization kinetics. Compared to polyolefins, the induced orientation of the chains is relatively weak.

Experimental Section

Instrumentation. SAXS was done using an in-house setup with a rotating anode X-ray generator (Rigaku RU-H300, 18 kW) equipped with two parabolic multilayer mirrors (Bruker, Karlsruhe), giving a highly parallel beam (divergence about 0.012°) of monochromatic Cu Kα radiation (wavelength λ = 0.154 nm). The SAXS intensity was collected with a two-dimensional gas-filled wire detector (Bruker Hi-Star). A semitransparent beamstop placed in front of the area detector allowed monitoring the intensity of the direct beam, to which the SAXS intensities were normalized.

* Corresponding author: e-mail liangbin@amolf.nl.

10.1021/ma0496145 CCC: $27.50 © 2004 American Chemical Society
Published on Web 06/19/2004

A Linkam CSS450 temperature-controlled shear system was employed as sample stage. The glass windows were replaced by two brass plates with apertures covered by 50 μm thick Kapton foil, allowing transmission of the X-ray beam. The PBT sample was held in the gap between the two windows and sheared by a single rotation step of the bottom plate. Because of the high experimental temperatures up to 250 °C, the Kapton windows were mechanically clamped onto the brass plates rather than glued. This also allowed to take the sample out without inducing deformations and to replace the windows easily.

Sample Treatment. PBT was provided by DSM Engineering Plastics (Arnite T08 200). The melting point was 225 °C, and the relative solution viscosity in *m*-cresol was 2.4. The number molecular weight and its distribution are 31 000 g/mol and 2, respectively. Plates with a size of 120 × 120 × 1.6 mm^3 were obtained by injection molding. The samples were preshaped into thin disks with a thickness of 1.0 mm and a diameter of about 30 mm in order to fit to the dimensions of shear cell. Before the actual measurements the sample was first melted at 240 °C, kept for 10 min, and then cooled to the crystallization temperature (198, 203, and 208 °C) at a cooling rate of 30 °C/min. Upon reaching the crystallization temperature, a step shear was applied with shear rates varying between 1 and 90 s^{-1} at shear strains of 1500% and 4500%, respectively. The whole process was monitored by SAXS using 30 s/frame.

Data Analysis. The two-dimensional SAXS intensity was first integrated azimuthally to obtain the scattering pattern as a function of $q = 4\pi \sin \theta/\lambda$, the modulus of the momentum transfer vector **q**, 2θ being the scattering angle. To examine the lamellar structures, linear correlation functions $\gamma(r)$ were calculated according to[39−41]

$$\gamma(r) = \frac{1}{Q}\int_0^\infty I(q)q^2 \cos(qr)\, \mathrm{d}q \qquad (1)$$

$$Q = \int_0^\infty I(q)q^2\, \mathrm{d}q \qquad (2)$$

where Q is the so-called invariant. As the final orientation of the samples was very weak (less than 2%), a Lorentz correction was applied. The correlation functions contain the basic morphological information for a model of lamellar stacks. The long spacing L can be estimated from the position of the first maximum. Further analysis of $\gamma(r)$ yields the average crystalline lamellar thickness l_c and the amorphous layer thickness l_a, with $L = l_c + l_a$. From these results the linear crystallinity $\phi_{cl} = l_c/L$ within the stacks can be calculated. However, analysis of the correlation function alone cannot tell which subspacing value belongs to l_c and which to l_a. In agreement with Hsiao et al.,[38] we assign the larger one to l_c. For an alternative assignment the linear crystallinity ϕ_{cl} can be smaller than the apparent crystallinity, which is unlikely.

The crystallization kinetics has been described using the half-time of crystallization as well as the Avrami equation.[42] The Avrami exponent n can be obtained through the general form

$$1 - X_s = \exp(-kt^n) \qquad (3)$$

where k is the rate constant of the crystallization process and X_s is the crystallinity defined by $X_s(t) = X_w(t)/X_w(\infty)$, in which X_w is the normalized crystallinity from the SAXS invariant. The Avrami exponent n provides information about the dimensionality of the growing crystalline material. At quiescent conditions spherulitic growth gives $n \approx 3$; larger values are found for a fiber nucleation model.[3]

An orientation parameter has been defined experimentally as follows. Figure 1 shows a typical two-dimensional SAXS pattern, from which two quadrants are chosen to represent the behavior along the meridian and equator, respectively. The integrated intensities in these two directions are designated as I_{me} and I_{eq}, respectively. Subsequently, we define the orientation parameter P_{or} as

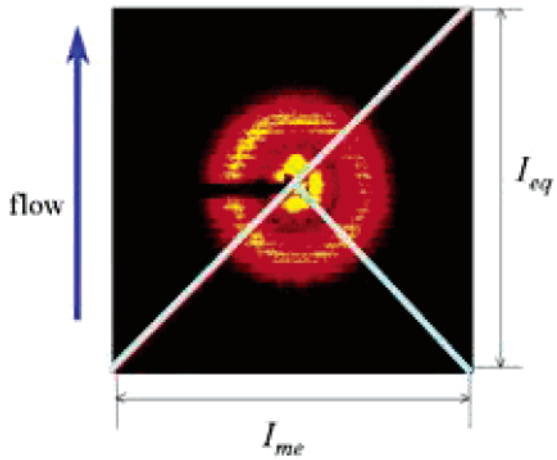

Figure 1. Schematic picture defining I_{eq}, I_{me}, and the orientational parameter P_{or}.

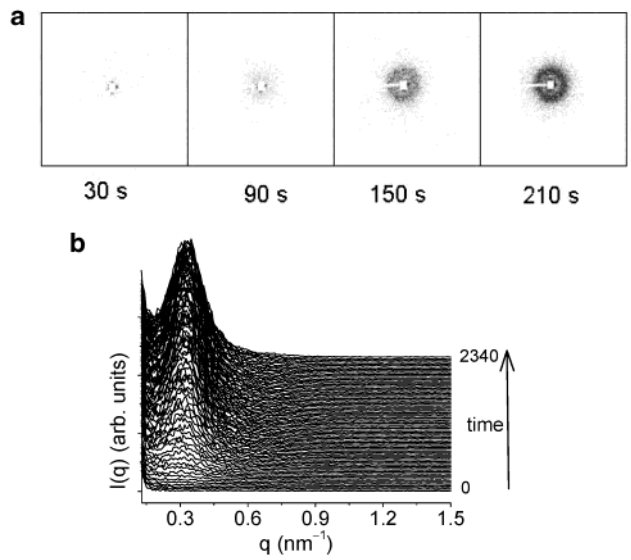

Figure 2. Crystallization at 203 °C after a step shear with a shear rate of 3 s^{-1} and a strain of 1500%: (a) typical two-dimensional SAXS and (b) one-dimensional SAXS.

$$P_{or} = \frac{I_{me} - I_{eq}}{I_{me} + I_{eq}} \qquad (4)$$

Atomic Force Microscopy. Atomic force microscopy (AFM) measurements were carried out with a Solver SFA (NT-MDT, Zelenograd, Moscow) in the tapping mode using a scanning cantilever. In this mode the AFM contrast of the phase image is due to different mechanical properties of the crystalline and the amorphous regions. To obtain fresh surfaces, the crystallized samples were cooled, taken out from the shear cell, and cut using a homemade cryogenic cutting setup. We prefer this approach above transmission electron microscopy because no staining is required, and moreover no sample damage occurs during the measurements.

Results

Figure 2a shows a series of four typical two-dimensional SAXS patterns of crystallization after a step shear. Only at the very beginning a clear orientation effect is seen, which is much weaker than for isotactic polypropylene under similar circumstances.[4−26] Figure 2b gives the corresponding azimuthal integrated one-

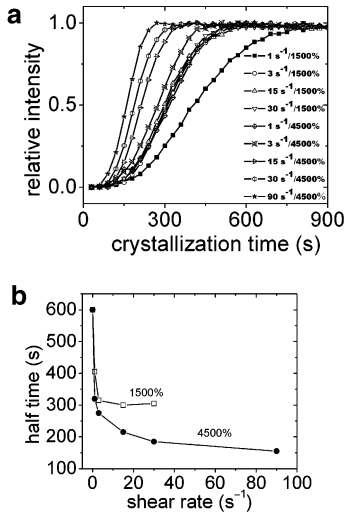

Figure 3. (a) Relative SAXS intensity during crystallization at 198 °C after a step shear for different shear histories. (b) Corresponding plots of the half-time of crystallization vs shear rate.

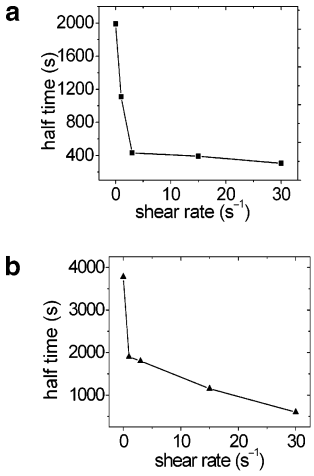

Figure 4. Half-time of crystallization vs shear rate (a constant strain of 4500%) at (a) 203 °C and (b) 208 °C.

dimensional SAXS patterns. With increasing crystallization time the SAXS peak shifts to slightly higher q values, similar as observed at quiescent conditions. This effect has been attributed to the insertion of lamellar crystals.[37]

Crystallization Kinetics. The crystallization kinetics can be further analyzed on the basis of the SAXS data. Figure 3a displays the relative SAXS intensity vs crystallization time for samples subjected to a different shear history at 198 °C. Both the shear rate and the shear strain promote the crystallization significantly. The half-time of crystallization, shown in Figure 3b, can be used to characterize the crystallization kinetics. Upon increasing the shear rate at a constant strain, the half-time of crystallization decreases, sharply reaching a saturation value of 3 s^{-1} for a strain of 1500%. At a strain of 4500% this point appears at a shear rate of about 15 s^{-1}. Evidently upon application of a shear field, in both cases a sharp decrease of the half-time is already obtained at relatively small shear rates. The influence of the shear field on the crystallization kinetics has also been studied at other two (higher) temperatures. Parts a and b of Figure 4 show the half-time of crystallization vs shear rate (constant shear strain of 4500%) at 203 and 208 °C, respectively.

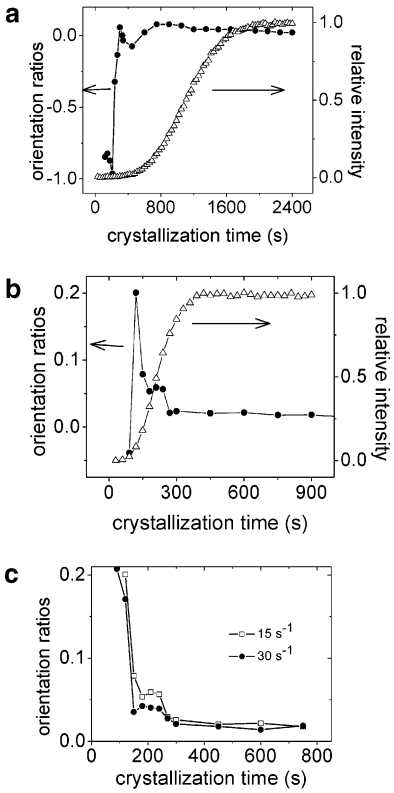

Figure 5. Evolution of orientation parameter with crystallization time at 203 °C after a step shear with a shear strain of 4500% and a shear rate of (a) 1, (b) 3, (c) 15, and 30 s^{-1}. For (a) and (b) the relative SAXS intensity is plotted for comparison.

Table 1. Avrami Exponent *n* of PBT Samples Crystallized at Different Temperatures after Subjected to a Different Shear History

shear rate (s^{-1})	shear strain (%)	N (198 °C)	N (203 °C)	n (208 °C)
0	0	3.1	3.5	3.4
1	1500	3.0		
3	1500	3.2		
15	1500	3.4		
30	1500	3.5		
1	4500	3.2	3.4	3.5
3	4500	3.4	3.3	3.4
15	4500	3.7	3.3	3.4
30	4500	3.9	3.3	3.1
90	4500	4.0		

The crystallization kinetics has been further analyzed by the Avrami model. Table 1 lists the Avrami exponent for PBT crystallization at the various temperatures and shear histories reported. At 198 °C application of a shear field leads to an increase of the Avrami exponent, but this effect does not show up at the higher temperatures studied.

Orientation. In general, shear imposes some orientation on the lamellar crystals, which is an important factor influencing the final properties. Parts a and b of Figure 5 show the orientation parameter P_{or} along with the crystallization time at 203 °C after a step shear with shear rate of 1 and 3 s^{-1}, respectively. For comparison, the integrated relative intensity is displayed in the same figure. For both shear rates the orientation parameter develops with time in a similar way. After the step shear has been applied, first P_{or} is negative, indicating a larger intensity in the equatorial direction than along the meridian. This can be interpreted as thread nucleation along the flow direction. During the second stage P_{or}

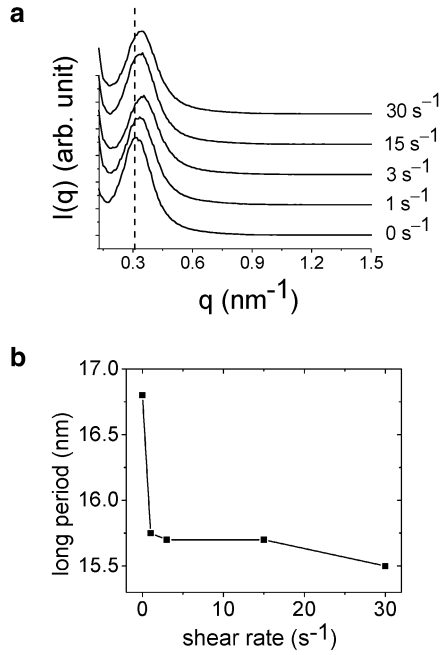

Figure 6. (a) One-dimensional SAXS patterns from crystallized samples after a step shear at 198 °C and (b) plot of long period vs shear rate, both for strain of 1500%.

changes sign from negative to positive. This demonstrates growth of the so-called kebabs for which the layer normal follows the flow direction, and the scattering intensity concentrates along the meridian. In the third stage P_{or} decreases sharply, as generally found for shear-induced crystallization of polymers: it indicates growth without any preferred orientation. During this decrease of P_{or} an interesting transition point occurs, indicating a slowing down of the process. Similar features are found also at larger shear rates (15 and 30 s^{-1}), as shown in Figure 5c. However, because of the faster growth process, now no negative value of P_{or} is observed at the beginning. At 198 and 208 °C, the evolution process of orientation parameter is similar to that at 203 °C. At 198 °C the orientation parameter at the beginning of crystallization is larger than the value at higher temperatures, but for all PBT samples crystallized after shear the final orientation is at the same level (less than about 2%).

Final Morphology. Figure 6a shows the final one-dimensional SAXS patterns from crystallized samples at 198 °C after a step shear. Figure 6b displays the corresponding long period vs shear rate: the application of shear clearly reduces the long period. A detailed analysis using correlation functions has been applied to samples crystallized at 203 °C. Parts a and b of Figure 7 show the final one-dimensional SAXS patterns and the corresponding one-dimensional density correlation function, respectively. The morphology parameters obtained from the correlation functions are plotted in Figure 7c. Similarly as at 198 °C, upon shearing the lamellar crystal period is reduced.

In addition to in-situ X-ray scattering, some ex-situ real-space investigations have been carried out on the shear-induced crystallized samples. Figure 8 shows a typical AFM phase image of a sample crystallized at 198 °C after a step shear. Taking the smearing effect of the tip size (radius of curvature about 15 nm) into account, the observed lamellar period is about 16 nm, in good agreement with the SAXS data that give 16.5 nm.

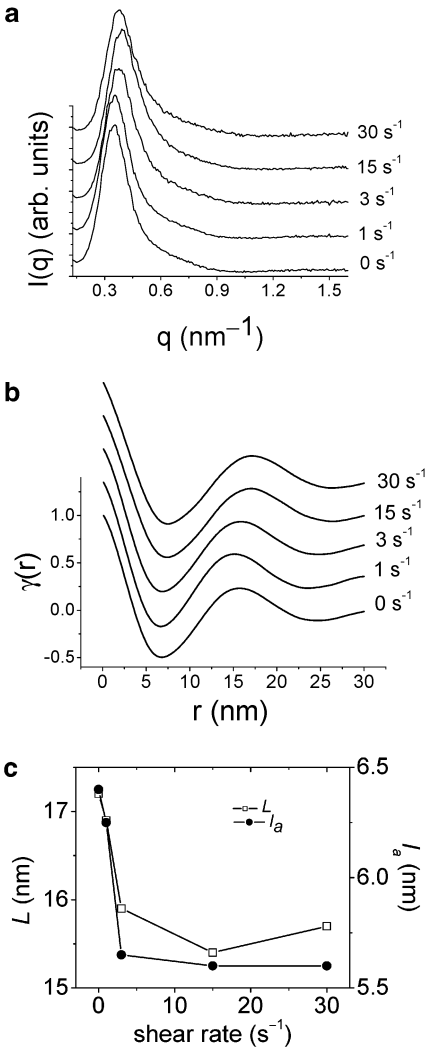

Figure 7. (a) One-dimensional SAXS patterns from samples crystallized at 203 °C after a step shear with a shear strain 4500%. (b) Corresponding one-dimensional density correlation functions. (c) Plot of long period and interlamellar amorphous thickness vs shear rate.

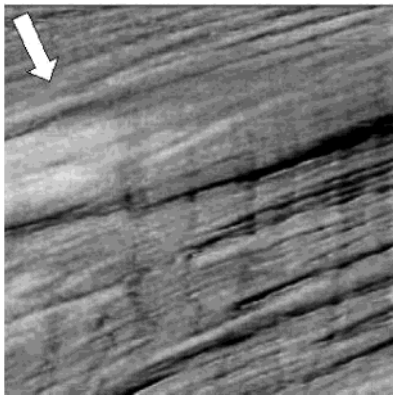

Figure 8. AFM phase image (0.8 × 0.8 μm^2) of a PBT sample crystallized at 198 °C after a step shear with shear rate of 3 s^{-1} and strain of 4500%. The arrow indicates the flow direction.

Discussion

Let us first consider the saturation of the crystallization rate as a function of shear rate (see Figures 3 and 4). Somani et al.[21] extended the idea of Keller and coworkers[43] for elongational flow-induced crystallization to shear flow. At a given shear rate, only molecules with

a chain length above a critical value M^* are supposed to be oriented. The oriented molecules serve as the precursor or primary nuclei. Here the molecular weight and its distribution play an essential role, and in a polydisperse polymer sample only the high-molecular-weight part contributes to the enhancement of the crystallization rate. Because $M^* \sim \dot{\gamma}^{-\alpha}$ ($\dot{\gamma}$ is the shear rate and α a positive exponent), the total number of oriented chains first increases with shear rate and then reaches a plateau. The observed saturation of the crystallization rate can be ascribed to this plateau of the amount of oriented chains.

The Avrami exponent for shear-induced crystallization of polymers can be much higher (~7) than that at quiescent conditions (~3).[44] This effect has been attributed to rodlike row nucleation. For PBT an increase of the Avrami exponent under the influence of shear is observed at 198 °C but not at higher crystallization temperatures. This means that row nucleation is not pronounced at 203 and 208 °C. Nevertheless, P_{or} shows at 203 °C a negative value just after shearing, which suggests that the shear field did induce row nuclei. The absence of a pronounced effect on the Avrami exponent can be attributed to a fast relaxation of the shear-induced row nuclei at the higher temperatures. Interestingly, the absence of row nucleation does not strongly influence the crystallization rate. Comparing the half-time of crystallization at quiescent conditions and after shear flow at the same crystallization temperature, the relative decrease is more significant at the higher temperatures. After a step shear with a rate of 30 s^{-1} and a strain of 4500%, the half-time of crystallization at 203 and 208 °C is about 15% of the half-time at quiescent conditions, while at 198 °C it is about 30%. These results imply that the crystallization kinetics is not directly coupled to the Avrami exponent. Nevertheless, the enhancement of the crystallization rate after shear must be due to an increased nucleation rate.

The idea of a microshish or point precursor[45] may be appropriate to explain the effect of the shear field. For a constant volume fraction of nuclei, we would expect a faster growth in a system with randomly dispersed small point precursors than in the case of long rod nuclei (linear aggregation of point precursors). The idea of point precursors is also in agreement with the results for P_{or}. Comparing the present situation to iPP, which is the most widely studied polymer with regard to this subject, the shear flow does not induce a strong orientation in PBT. The low orientation ratio does not support a shish-kebab or transcrystalline model in which crystal growth starts on the surface of row nuclei. Alternatively, point nuclei may play a dominated role in PBT. Commercially produced PBT has a shorter chain length as well as a smaller polydispersity than that of iPP, which are major factors explaining both the enhancement of the crystallization rate and the orientational order. The average length of PBT chains is only about 164 nm, while a normal commercial iPP has a chain length 1 order of magnitude longer. The polydispersity of PBT is 2, which is about half of the value of normal iPP materials. With narrow molecular weight distribution, both high- and low-molecular-weight iPP materials give a small orientation even after strong shear, which is similar to the result from PBT. Evidently, the polydispersity is an essential factor to control the orientation. The different behavior of PBT and iPP may originate from differences in their methods of synthesis. The shear-induced crystallization behavior of other polymers, such as PET, polyamides, etc., also synthesized with condensation polymerization, is expected to show similar features as PBT.

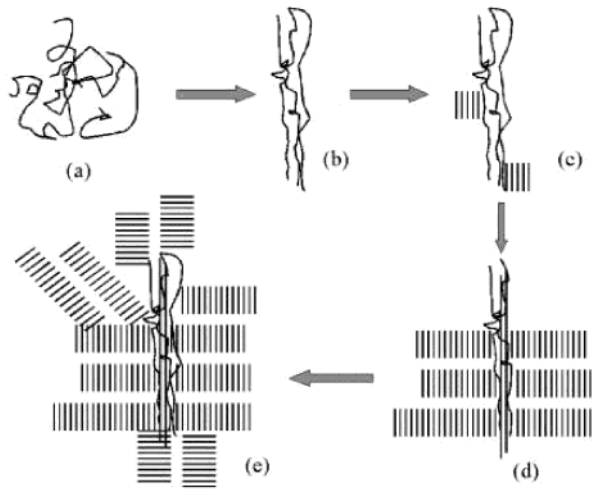

Figure 9. Schematic picture of the morphological development during shear-induced crystallization: (a) random coil before shear, (b) shear-induced row nucleus, and (c−e) epitaxial growth of kebabs.

The development of the orientation parameter P_{or} suggests a clear evolution of the morphology, which is schematically illustrated in Figure 9. Initially the polymer chains are in a random coil state (Figure 9a). After application of a step shear some of the chains keep a preferred orientation along the flow direction and create primary nuclei (Figure 9b). The anisotropic distribution of these nuclei leads to the negative value of P_{or} observed at this stage (see Figure 5). Figure 9c,d indicates the growth of kebabs, which results in strong scattering along the meridian: P_{or} changes to positive values. Finally, the majority of crystals have little preferred orientation, resulting in a small value of P_{or} in the final stage of the crystallized samples (Figure 9e).

The growth process in Figure 9 provides a general model for shear- or flow-induced crystallization, which is characterized by rodlike row nuclei parallel to flow direction. In the Avrami growth model the exponent n is expected to be larger than 3, as observed in PBT at 198 °C. To explain the growth process at 203 and 208 °C, we present another model (Figure 10) in which shear flow accelerates the crystallization kinetics but does not significantly influence the Avrami exponent. Compared to the model of Figure 9, the important difference is the incorporation of relaxation of the shear-induced row nuclei. The negative orientation parameter in Figure 6 indicates at 203 °C initially formation of rodlike row nuclei (see Figure 10b). Because shear-induced row nuclei do not result from a thermodynamic process, they always tend to relax. This process of breaking down rodlike row nuclei into several point precursors (Figure 10c) is expected to become increasingly important at higher temperatures. The subsequent growth of lamellar crystals from these point precursors leads to little preferred orientation. The slowing down of the crystal growth and the prolonged incubation time at high temperatures provides the row nuclei with the freedom in time and space to relax and to diffuse. For the same volume fraction of nuclei, the relative acceleration of the crystallization kinetics will be larger for the growth model of Figure 10 than for the general model of Figure

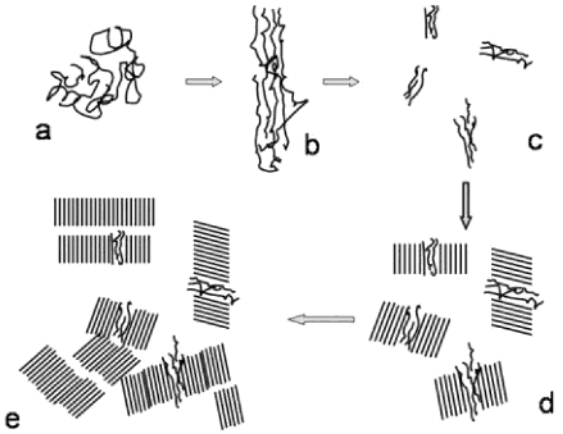

Figure 10. Schematic picture of the formation of primary point nuclei and the subsequent epitaxial crystal growth: (a) random coil before shear, (b) shear-induced row nuclei, (c) formation of primary point nuclei due to relaxation of the row nuclei, and (d, e) epitaxial growth of kebabs.

9, even though in the former model the Avrami exponent is not affected. We believe that the growth approach of Figure 10 can be generally applied to polymers crystallizing after shear at small supercooling.

Despite the large amount of work on shear-induced crystallization, to the best of our knowledge no influence of shear on the lamellar thickness has been reported so far. Morphological observations usually concentrate on the orientation of the lamella and the density of nuclei leading to spherulites. We observe for PBT a decrease of the long period with shear, which effect parallels the decreasing half-time of crystallization. One possible reason might be the high nucleation density on the microshish, which could bring down the long period. This suggests a possible connection between the lamellar orientation and the reduction of the long period because both are determined by the same lamellar stacks formed around the primary nuclei. The reduction of the lamellar spacing is about 6−8%, which is appreciably larger than the orientation ratio (≤2%). This difference suggests that the influence of shear field manifests not only through the nucleation but also through the growth process.

Conclusions

The shear-induced crystallization behavior of PBT has been studied by in-situ SAXS and WAXS. As generally found for shear-induced crystallization of polymers, both the shear rate and the shear strain enhance the crystallization rate, while saturation occurs for large shear rate. With increasing shear strain, this point appears at a higher shear rate. At a temperature of 198 °C, the shear field leads to an increase of the Avrami exponent, but not at higher temperatures (203 and 208 °C). Both the Avrami exponent and the low degree of orientation point to a microshish or point-precursor model to describe the shear-induced crystallization behavior of PBT at high temperatures. The formation of the point precursors is attributed to a relaxation of the shear-induced row nuclei during the incubation time for crystallization. Finally, the shear field leads to a pronounced reduction of the long period.

Acknowledgment. The authors thank Dr. M. van Gurp and Dr. W. Gabrielse (DSM) for providing the materials and valuable discussions. This work is part of the Softlink research program of the "Stichting voor Fundamenteel Onderzoek der Materie" (FOM), which is financially supported by the "Nederlandse Organisatie voor Wetenschappelijk Onderzoek" (NWO).

References and Notes

(1) Nakatani, A. I.; Dadmun, M. D. *Flow-Induced Structure in Polymers*; American Chemical Society: Washington, DC, 1995.
(2) Muthukumar, M. *Eur. Phys. J. E* **2000**, *3*, 199.
(3) Miller, R. L. *Flow-Induced Crystallisation in Polymer Systems*; Gordon and Breach Science Publishers: New York, 1979.
(4) Kumaraswamy, G.; Issian, A. M.; Kornfield, J. A. *Macromolecules* **1999**, *32*, 7537.
(5) Nogales, A.; et al. *Polymer* **2001**, *42*, 5247.
(6) Jerschow, P.; Janeschitz-Kriegel, H. *Int. Polym. Proc.* **1997**, *7*, 72.
(7) Kornfield, J. A.; Kumaraswamy, G.; Issaian, A. M. *Ind. Eng. Chem. Res.* **2002**, *41*, 6383.
(8) Seki, M.; Thurman, D. W.; Oberhauser, J. P.; Kornfield, J. A. *Macromolecules* **2002**, *35*, 2583.
(9) Kumaraswamy, G.; Verma, R. K.; Issian, A. M.; et al. *Polymer* **2000**, *41*, 8931.
(10) Monasse, B. *J. Mater. Sci.* **1992**, *27*, 6047.
(11) Jay, F.; Haudin, J. M.; Monasse, B. *J. Mater. Sci.* **1999**, *34*, 2089.
(12) Rawson, K. W.; Allan, P. S.; Bevis, M. *J. Polym. Eng. Sci.* **1999**, *39*, 177.
(13) Chen, L. M.; Shen, K. Z. *J. Appl. Polym. Sci.* **2000**, *78*, 1906.
(14) Vleeshouwers, S.; Meijer, H. E. H. *Rheol. Acta* **1996**, *35*, 391.
(15) Boutahar, K.; Carrot, C.; Guillet, J. *Macromolecules* **1998**, *31*, 1921.
(16) Nagatake, W.; Takahashi, T.; Masubuchi, Y.; et al. *Polymer* **2000**, *41*, 523.
(17) Hosier, I. L.; Bassett, D. C.; Moneva, I. T. *Polymer* **1995**, *36*, 4197.
(18) Garcia-Gutierrez, M. C.; Alfonso, G. C.; Riekel, C.; Azzurri, F. *Macromolecules* **2004**, *37*, 478.
(19) Somani, R. H.; Yang, L.; Hsiao, B. S. *Physica A* **2002**, *304*, 145.
(20) Ran, S. F.; Zong, X. H.; Fang, D. F.; Hsiao, B. S.; Chu, B.; Philips, R. A. *Macromolecules* **2001**, *34*, 2569.
(21) Somani, R. H.; Hsiao, B. S.; Nogales, A.; et al. *Macromolecules* **2000**, *33*, 9385.
(22) Somani, R. H.; et al. *Macromolecules* **2002**, *35*, 9096.
(23) Elmoumni, A.; Winter, H. H.; Eaddon, A. J.; Fruitwala, H. *Macromolecules* **2003**, *36*, 6453.
(24) Nogales, A.; Mitchell, G. R.; Vaughan, A. S. *Macromolecules* **2003**, *36*, 4898.
(25) Li, L. B.; de Jeu, W. H. *Macromolecules* **2003**, *36*, 4862.
(26) Li, L. B.; de Jeu, W. H. *Faraday Discuss.* **2004**, *218*.
(27) Myung, H. S.; Yoon, W. J.; Yoo, E. S.; Kim, B. C.; Im, S. S. *J. Appl. Polym. Sci.* **2001**, *80*, 2640.
(28) Yoon, W. J.; Myung, H. S.; Kim, B. C. *Polymer* **2000**, *41*, 4933.
(29) Blundell, D. J.; Mahendrasingam, A.; Martin, C.; Fuller, W.; Mackerron, D. H.; Harvie, J. I.; Oldman, R. J.; Riekel, C. *Polymer* **2000**, *41*, 7793.
(30) Schultz, J. M.; Hsiao, B. S.; Samon, J. M. *Polymer* **2000**, *41*, 8887.
(31) Penning, J. P.; van Ruiten, J.; Brouwer, R.; Gabrielse, W. *Polymer* **2003**, *44*, 5869.
(32) Dimitrakopoulos, P.; Brady, J. F.; Wang, Z. G. *Phys. Rev. E* **2001**, *64*, 050803.
(33) Shimada, T.; Doi, M.; Okano, K. *J. Chem. Phys.* **1988**, *88*, 2815.
(34) Stein, R. S.; Misra, A. *J. Polym. Sci., Polym. Phys. Ed.* **1980**, *18*, 327.
(35) Matsuo, M.; Gesgi, K.; Sawatari, C. *Macromolecules* **1982**, *15*, 193.
(36) Cheng, S. Z. D.; Pan, R.; Wunderlich, B. *Macromol. Chem.* **1988**, *189*, 2443.
(37) Hou, P. P.; Cebe, P.; Capel, M. *J. Polym. Sci., Polym. Phys. Ed.* **1992**, *30*, 1459.
(38) Hsiao, B. S.; et al. *Polymer* **1999**, *40*, 3515.
(39) Vonk, C.; Kortleve, G. *Kolloid Z. Z. Polym.* **1967**, *220*, 19.
(40) Strobl, G. R.; Schneider, M. *J. Polym. Sci., Polym. Phys. Ed.* **1980**, *18*, 1343.
(41) Goderis, B.; Reynaers, H.; Koch, M. H. J.; Mathot, V. B. F. *J. Polym. Sci., Part B: Polym. Phys.* **1999**, *37*, 1715.
(42) Wunderlich, B. *Macromolecular Physics*; Academic Press: New York, 1976; Vol. 2.

(43) Keller, A.; Kolnaar, H. W. H. *Mater. Sci. Technol.* **1997**, *18*, 189.
(44) Sherwood, C. H.; Price, F. P.; Stein, R. S. *J. Polym. Sci., Part C: Polym. Symp.* **1982**, *63*, 77.
(45) Janeschitz-Kriegl, H.; Ratajski, E.; Wippel, H. *Colloid Polym. Sci.* **1999**, *277*, 217.

MA0496145